Localization of arrhythmogenic sites in post-ischemic ventricular tachycardia using Network Granger Causality.

Lucas Zoroddu[1,2], Pierre Humbert[3], Laurent Oudre[1], Thomas Demarcy[2], Laurent Launay[2], Francis Bessière[4]

***Abstract*— Detecting abnormal electrical wave propagation in Sinus Rhythm (SR) in patient with Ventricular Tachycardia (VT) can enhance treatment strategies. However, traditional methods, like activation maps, often produce biased results due to the difficulty of calculating what is called Local Activation Time (LAT). This paper introduces a method based on Network Granger Causality (NGC) to assess VT mechanics. Instead of computing LATs, NGC generalizes the binary Granger causality framework and allows to leverage the EGM morphologies, identifying temporal causality links within a network of electrograms. Furthermore, by incorporating geometrical information in the NGC model, we improved the interpretation of causal relationships and applied our method to localize anomalies via the reconstruction error computation. Using simulated clinical data, we compare our method to standard techniques, such as voltage and velocity computation. Our results show that NGC-based analysis improves VT anomaly detection during SR over standard methods in terms of ROCAUC, increasing performance from 0.80–0.85 to 0.89. Finally, we present an example on a real patient with VT.**

I. Introduction

Cardiac arrhythmias, such as fibrillation and tachycardia (atrial or ventricular), are common and associated with a high risk of mortality. Although drugs may be sufficient to eliminate the pathology, in some cases it is necessary to perform a surgical procedure, during which intracardiac electrocardiograms are recorded. In the literature, researchers often investigate the use of these electrocardiograms to understand the propagation patterns of depolarization wavefronts in the heart, potentially detecting pathological substrates related to arrhythmias. The most common method to understand cardiac activation dynamics relies on the accurate determination of the Local Activation Times (LATs) from recorded intracardiac electrograms (EGMs) which mark the moment when depolarization reaches specific electrodes. However the computation of these LATs is a non-trivial task and existing methods can return very different results (see e.g. [1]). Moreover, most of these methods rely on univariate signal analysis, treating each electrogram independently. This can be suboptimal since our objective is to capture a global phenomenon that can be observed through the links between electrograms. More recently, some works have proposed methods to detect temporal causality relationships between intracardiac activity signals [2], [3], [4]. For example, in [2], a Granger causality-based method was proposed to localize the sites, called drivers, that can cause a ventricular fibrillation. However, this method consider pairwise causality tests, which have been shown to have important limitations [5]. Another limitation of this method is its sensitivity to neighborhood selection, as causality tests are conducted only among signals within predefined spatial neighborhoods.

Contributions: To address these limitations, this work investigates the use of the Network Granger Causality (NGC), a generalization of the Granger causality, to capture anomalies in the wave propagation when the patient is in sinus rhythm (i.e not under Ventricular Tachycardia (VT)). More specifically, we first introduce a NGC-based algorithm enabling the capture of electrical wave dynamics from recorded EGMs and distances between electrodes. This method allows to infer causality links between nearby EGMs, without manually selecting a neighborhood, and to reconstruct the inputs signals as linear combinations of the others with some delays. Then, we use the EGMs reconstruction error to automatically detect anomalies in the propagation, potentially leading to the identification of the sites responsible of the tachycardia. Finally, we show the efficiency of our methodology through simulated data and we present an example on a real patient.

II. Method

A. Preliminaries

In order to define the NGC, we first recall the concept of Granger causality between two signals [6]. Let x and y be two 1D signals such that at time $t = 1, 2, \ldots$:

$$y[t] = \sum_{i=1}^{d} \alpha_i y[t-i] + \sum_{i=1}^{d} \beta_i x[t-i] + \varepsilon[t] \,, \tag{1}$$

where $\varepsilon[t] \sim \mathcal{N}(0, \sigma^2)$ for $\sigma > 0$, $d \geq 1$ is the order of the model, and $\{\alpha_i, \beta_i\}_{i=1}^{d}$ are parameters. We say that x Granger-causes y if one of the $\{\beta_i\}_i$ is non zero. In practice, as $\{\alpha_i, \beta_i\}_{i=1}^{d}$ are unknown, we estimate them by minimizing the least square error between the observed signal y and its reconstruction using x and Model (1). To generalize the Granger causality to multiple 1D signals, the NGC

*[1] Université Paris Saclay, Université Paris Cité, ENS Paris Saclay, CNRS, SSA, INSERM, Centre Borelli, F-91190, Gif-sur-Yvette, France.
*[2] Volta Medical, Marseille, France.
*[3] Laboratoire de Mathématiques d'Orsay, Orsay, France.
*[4] Hôpital Cardiologique Louis Pradel, Hospices Civils de Lyon, France, Université Claude Bernard Lyon 1, INSERM - LabTau – Unit 1032, Lyon, France.

framework was built on the following VAR(d) model:

$$X[t] = \sum_{\tau=1}^{d} \mathbf{C}^{\tau} X[t-\tau] + \varepsilon[t] \,, \tag{2}$$

where $X[\cdot] = (X_1[\cdot], ..., X_p[\cdot])$ is a p-dimensional signal, d is the order of the VAR, $\{\mathbf{C}^{\tau}\}_{\tau=1}^{d}$ are matrices in $\mathbb{R}^{p\times p}$ encoding causality links between the different dimensions of the signal at each time $t = 0, 1, \ldots, T$, and $\varepsilon[t] \sim \mathcal{N}(0, \sigma^2 I_p)$ is some noise where $\sigma > 0$ and I_p the identity matrix of size $p \times p$.

As for Model (1), in practice, given N samples $X^{(n)}[t] \in \mathbb{R}^p$ with $n = 1, ..., N$ and $t = 0, \ldots d$, one possibility to estimate the parameters $\{\mathbf{C}^{\tau}\}_{\tau=1}^{d}$ is to maximize the likelihood of Model (2). This leads to the following least square problem:

$$\min_{\mathbf{C}^1,\ldots,\mathbf{C}^d} \frac{1}{2N} \left\| \mathbf{X}[d] - \sum_{\tau=1}^{d} \mathbf{C}^{\tau} \mathbf{X}[d-\tau] \right\|_F^2 , \tag{3}$$

where $\|\cdot\|_F$ is the Frobenius norm and $\mathbf{X}[t] \in \mathbb{R}^{p\times N}$ is the matrix storing all the $\{X^{(n)}\}_{n=1}^{N}$ in column. As shown in [7], this minimisation can be divided into p independent sub-problems, which are easier to handle, and we can add some penalization term to improve the parameters inference. For $j = 1, ..., p$, these sub-problems are given by:

$$\min_{\mathbf{C}^1_{j:},\ldots,\mathbf{C}^d_{j:}} \frac{1}{2N} \left\| \mathbf{X}_j[d] - \sum_{\tau=1}^{d} \mathbf{C}^{\tau}_{j:} \mathbf{X}[d-\tau] \right\|_2^2 + \lambda \cdot \mathscr{P}(\mathbf{C}^1_{j:}, ..., \mathbf{C}^d_{j:}) \,, \tag{4}$$

with $\lambda \geq 0$ a hyper parameter and $\mathscr{P}(\cdot)$ a penalization term.

B. Method formulation

The goal of our method is to compute causality links between EGMs recorded by electrodes at several locations. To this end, we rely on the NGC model (2) which allows to (automatically) compute causality links between a set of p electrodes (i.e. the matrices $\{\mathbf{C}^{\tau}\}_{\tau=1}^{d}$). Furthermore, since the electrical wave propagation is governed by reaction diffusion equations, we propose to leverage that the nearest the recording electrodes, the most likely the causality link, by adding to Model (2) this spatial information through the penalization term. In detail, we first compute the pairwise distances matrix between electrode positions and apply a Gaussian kernel to obtain a matrix $\mathbf{W} = \left[K_\rho(\delta(p_i, p_j))\right]_{1\leq i,j\leq p}$, where δ is a distance, p_i are the recording positions and $K_\rho : x \mapsto \exp(-x^2/\rho^2)$. Note that the matrix $\mathbf{W}$ contains values between 0 and 1, and the higher the value, the nearest the electrode positions. Finally, we replace $\mathscr{P}(\cdot)$ in (4) by the following adaptive lasso penalty:

$$\mathscr{P}(\mathbf{C}^1_{j:}, \ldots, \mathbf{C}^d_{j:}) = \sum_{\tau=1}^{d} \sum_{j=1}^{p} \frac{|\mathbf{C}^{\tau}_{i,j}|}{\mathbf{W}_{i,j}} \,. \tag{5}$$

This penalty encourages sparsity while incorporating geometrical constraints through $\mathbf{W}$ [8]. In addition, following the work in [9], we allow refinement of the prior matrix $\mathbf{W}$ through iterations using an alternating minimization framework (sequently updating $\mathbf{C}$ then $\mathbf{W}$). This is done by solving the following optimization problem:

$$\begin{aligned} \min_{\mathbf{W}', \mathbf{C}^1,\ldots,\mathbf{C}^d} \; & \frac{1}{2N} \sum_{n=1}^{N} \left\| X^{(n)}[d] - \sum_{\tau=1}^{d} \mathbf{C}^{\tau} X^{(n)}[d-\tau] \right\|_2^2 \\ & + \lambda \sum_{\tau=1}^{d} \sum_{1\leq i<j\leq p} \frac{|\mathbf{C}^{\tau}_{i,j}| + |\mathbf{C}^{\tau}_{j,i}|}{\mathbf{W}'_{i,j}} \\ & + 2\lambda \sum_{1\leq i<j\leq p} \log(2\mathbf{W}'_{i,j}) + \gamma \left\| \mathbf{W}' - \mathbf{W} \right\|_F^2 \end{aligned} \tag{6}$$

$$\text{s.t. } \mathbf{W}'_{i,j} \geq 0 \,,\, \mathbf{W}'_{i,j} = \mathbf{W}'_{j,i} \;,\; 1 \leq i < j \leq p \,,$$

where λ and γ are hyper parameters and $\mathbf{W}$ is the initial computed prior matrix. When $\mathbf{W}'$ is fixed, Problem (6) reduces to Problem (4) and can be easily solved using the package cvxpy [10]. Furthermore, when $\mathbf{C}$ is fixed, the associated problem can be solved as explained in [9]. The intuition here is that $\mathbf{W}$ encodes our prior knowledge (the closest the recording electrodes, the most likely the causality link), but it could be noisy or erroneous and lead to biased results due to an irrelevant penalization. Thus, refining the prior matrix through iterations (taking into account information learned at the previous iteration) leads to a more accurate penalization in the optimization problem and results in a better reconstruction of the true underlying causal links.

C. Anomaly detection with NGCE

Using the d matrices $\{\mathbf{C}^{\tau}\}_{\tau=1}^{d}$ returned by Problem (6), we can construct d causal graphs (one for each lag) that give insights about the global propagation of the signals. Furthermore, we can compute the reconstruction NGC Error (NGCE) of the j-th EGM defined by:

$$NGCE_j = \frac{1}{T-d+1} \sum_{t=d}^{T} \left(X_j[t] - \sum_{\tau=1}^{d} \left(\mathbf{C}^{\tau} X[t-\tau]\right)_j \right)^2 . \tag{7}$$

This error has already proved its efficiency to automatically detect anomalies [11]. The intuition is that we are looking for abnormal signals relative to its neighborhood, so the 'unpredictability' of a particular EGM given its neighbor EGMs is a good indicator of anomaly. The full procedure is summary in Algorithm 1.

Algorithm 1

Inputs: EGMs data $\mathbf{Y} \in \mathbb{R}^{p\times T}$, electrode positions p_i, hyperparameters $(\lambda, \gamma, \rho, d)$
Output: Reconstruction errors $E_1, \ldots, E_p$

1: Compute distance matrix D using Euclidean distance between each pair of electrode.
2: Compute prior matrix $\mathbf{W} \leftarrow \exp(-D^2/\rho^2)$
3: Transform $\mathbf{Y}$ into N successive overlapping segments of size d: $\mathbf{X} = (\mathbf{Y}[0:d], \mathbf{Y}[1:d+1], ..., \mathbf{Y}[T-d:T])$.
4: Solve the optimization problem (6) following [9]
5: Compute the reconstruction errors $NGCE_1, \ldots, NGCE_p$

III. Experiments

In this section, we use our method to localize pathological areas in the ventricle, and more specifically isthmus and areas of slow conduction from EGM signals. We compare ourselves to voltage and velocity computation, which are the two standard approaches to localize pathological tissues. Indeed, in practice, low-voltage areas or low-velocity are often targeted, as they are good indicators of the presence of scars where the electricity cannot propagate properly. However, note that the conduction velocity is not trivial to estimate from EGMs, especially in pathological ventricles. Actually, as discussed in [12], the conduction velocity computation is a difficult problem and there are several methods to estimate it. In our experiments, we have computed the conduction velocity using the following procedure: (1) estimation of the LAT by computing $\arg\max dV/dt$ for each EGM, (2) interpolation on the full surface using radial basis functions (Gaussian kernel), (3) computation of the LAT gradient norm inverse to obtain the velocity (see [12] for more details). Moreover, since the LAT estimation depends a lot on the method used, we have also compared our method to the velocity computation using true LATs (available for simulated data).

In summary, we compared four methods:

1) **NGCE**: the method presented in Section II.
2) **V_estimated**: Velocity computation using a standard LAT estimator.
3) **V_true**: Velocity computation using the true LATs.
4) **Voltage** computation.

A. Synthetic data

– Simulation procedure. We perform a quantitative analysis using simulated clinical EGM signals following the approach proposed in [13]. This approach has also been used in several research papers (see e.g. [14], [15]). First, the ventricle tissue is modeled by a two-dimensional grid of size 300×300 on which we generate random patterns of scars and isthmus. Then, we simulate the electrical wave propagation of a given action potential in the tissue by solving the Eikonal equation. On top of this grid, we add another grid of size 14×14 indicating the position of 196 electrodes. Finally, we compute a spatial convolution of the potentials to simulate the electrode recordings. An illustration of the simulated EGM signals is given in Figure 1 (bottom panel). For more details, we refer to [13].

To obtain a wide variety of conductivity scenarios, we randomly generated 110 conduction velocity maps by performing dilation, rotations and translations of 5 manually built patterns of scars and slow conduction areas. An example of one of these maps is shown in Figure 1 (top left panel). Then, we simulated the EGMs as explained above and we labeled as 'abnormal' all the 300×300 grid cells with a low (but non zero) conduction velocity. In these experiments, we set ρ to the median of the pairwise

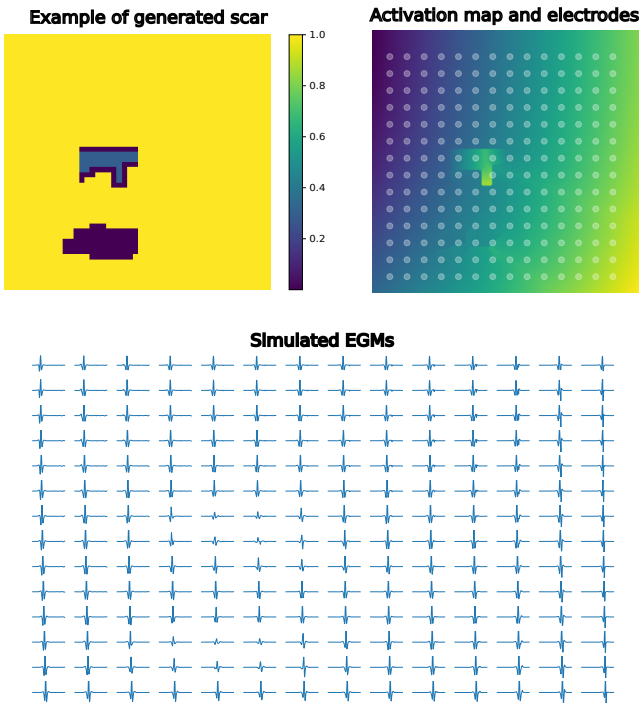

Fig. 1. Example of simulated data used for experiments. **Top left panel:** True velocity map with a dense scar area and an isthmus. **Top right panel:** Associated activation map obtained solving the Eikonal equation and electrodes positions (blue points). **Bottom:** Generated EGMs. Note that only these EGMs are available and the two maps are not part of the input data.

distance between the electrodes, 10 samples were used to select the hyperparameters (d, λ, γ) of our method and we ran the experiments using the 100 other samples.

– Metrics. Recall that the task is to retrieve the slow conduction areas on the tissue (i.e. on the 300×300 grid) taking as inputs only the simulated EGMs and the sensors locations. Since our method and the voltage computation only return values for each electrode, we performed an interpolation using the Nadaraya method [16] to obtain a real value for each cell of the tissue. As we are interested in evaluating whether the features (NGCE, velocity, voltage) are relevant for separating healthy areas from abnormal ones, we computed the ROCAUC [17]. This indicates the capacity of the different methods to detect abnormal cells and thus potential sites responsible of the tachycardia.

– Results. A visualization of the features NGCE, velocity, and voltage returned by each method on the example of Figure 1 is given in Figure 2. Furthermore, the values of the ROCAUC metric obtained with the four methods on the 100 samples are given in table I (the larger the better). In addition, to highlight that our method can identify abnormal areas regardless of the size of the scars, we have divided them into two categories: small scars and large scars (corresponding respectively to the smaller 25% and the other ones). First, on the ROCAUC metric, our method NGCE

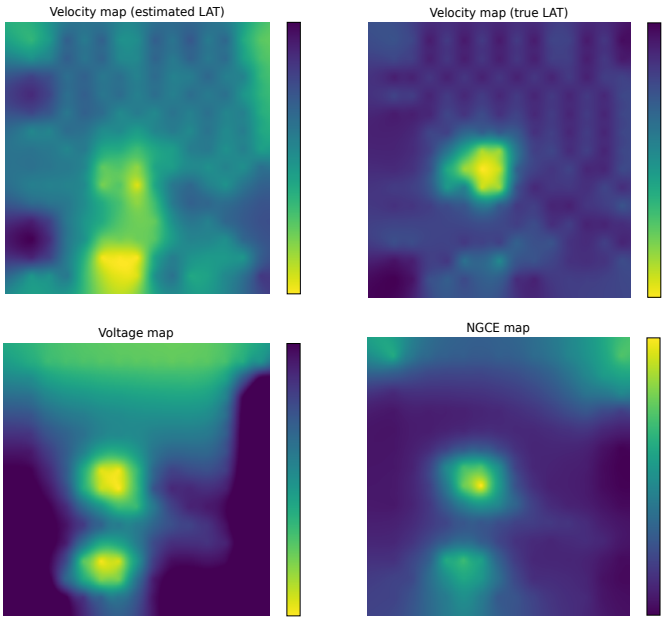

Fig. 2. Example of results obtained with simulated data. Note that this example is obtained using the case presented in Figure 1.

outperforms the standard approaches achieving a score of 0.89 (against 0.8 and 0.85 for voltage and velocity) for all type of scars. Remarkably, NGCE even returns better results that the velocity computation using true LATs, while we are interested to detect areas with slow velocity. Note also that, as expected, all methods better identify large scars rather than the small ones, but NGCE remains superior in both scenarios. One explanation behind the high performance of our method is the following: wave propagation anomalies often result in local abnormal potentials in the signals, making them difficult to be reconstructed using neighborhood signals, which is exactly what is computed by NGCE.

Method/ROCAUC	All Scars	Small Scars	Large Scars
NGCE	**0.89** $\pm$ 0.13	**0.84** $\pm$ 0.15	**0.95** $\pm$ 0.07
V_estimated	0.80 $\pm$ 0.20	0.73 $\pm$ 0.22	0.90 $\pm$ 0.10
V_true	0.86 $\pm$ 0.22	0.81 $\pm$ 0.24	0.91 $\pm$ 0.16
Voltage	0.85 $\pm$ 0.12	0.79 $\pm$ 0.12	0.93 $\pm$ 0.08

TABLE I
ROCAUC SCORES WITH STANDARD DEVIATIONS FOR ALL SCARS, SMALL SCARS, AND LARGE SCARS.

B. An example on a real patient

Finally, we tested our method on real data recorded during an ablation procedure.

– Data Extraction. The procedure was performed on a post-ischemic VT patient at the Saint-Joseph Clinique (Marseille, France) using the EnsiteX mapping system. Unipolar EGMs and electrode locations were acquired with an HDGrid catheter of 16 electrodes during sinus rhythm (at a sampling frequencies of 1000 Hz for the EGMs and 100Hz for the positions). The goal of this ablation procedure was to identify arrhythmogenic sites (i.e., isthmus and slow conduction areas) and ablate them. In practice, the physicians introduce a catheter equipped with electrodes which they move around to record signals throughout the ventricle. The 3D ventricle geometry and ablation tags (blue points in Figure 4) were collected, serving as ground truth for qualitative evaluation. All data were extracted in compliance with the General Data Protection Regulation (GDPR).

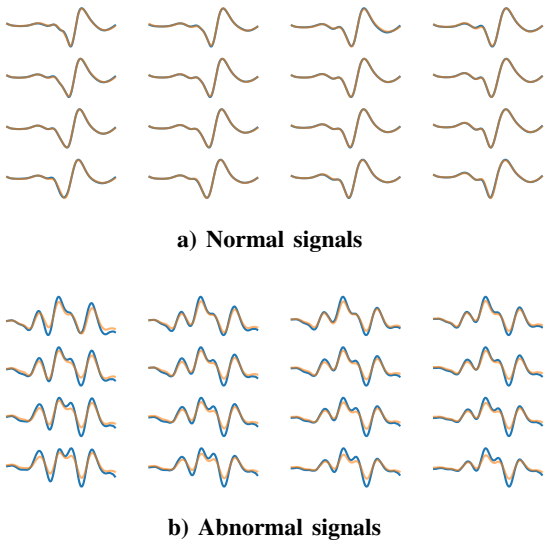

Fig. 3. Two segments recorded by the 16 electrodes of the HDGrid catheter. In blue the true signals and in orange the reconstruction with our method.

– Data Processing. Recall that the raw signals consisted of continuous recordings of two time series per electrode (16 electrodes in total): the unipolar signal and the 3D location time series. We extracted all 2.5-second segments where the catheter remained stable, resulting in a data set of $N_s = 200$ segments, each containing 16 unipolar signals and corresponding electrode positions. Our method was then applied to each segment, and the computed values were projected onto the 3D ventricle geometry. Finally, we performed Nadaraya interpolation to cover the entire ventricle.

– Results. Figure 3 displays two examples of signals reconstructed with our method when the segments are normal (upper panel) or abnormal (lower panel). As expected, abnormal signals are less well reconstructed, which means that their NGCEs are greater than those of normal signals. In addition, we display in Figure 4 the values of the NGCE (top panel) or voltage (bottom panel) projected on the 3D ventricule. It should be noted that computing conduction velocity is a very difficult task for real data, and the results obtained were very poor. We therefore only present the visualization of outputs for NGCE and voltage computation. We can see on Figure 4 that, although the voltage maps correlate well with the ablation sites (all tags, i.e. blue points,

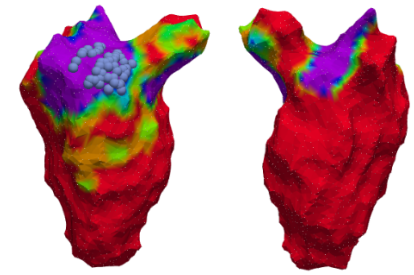

a) NGCE map

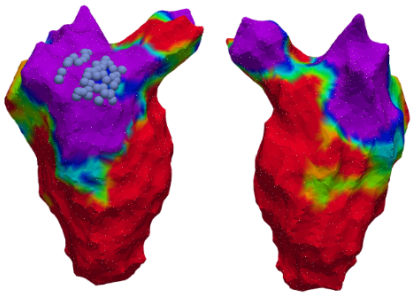

b) Voltage map

Fig. 4. Example of voltage and NGCE map on real data with ablation set. The color range goes from red to purple: red indicates a normal area while purple indicates the most abnormal sites. More precisely, purple areas correspond to small voltage areas and large NGCEs.

lie in low-voltage areas indicated by the purple color), they lack precision compared with the NGCE map. Notably, the NGCE map shows the greatest overlap between the purple regions (indicating high NGCE values) and the ablation labels, highlighting its superior accuracy for this particular patient.

IV. Conclusion

In this paper, we have introduced a methodology to automatically detect arrhythmogenic sites in post-ischemic ventricular tachycardia from electrograms (EGMs). Our method is based on Network Granger Causality (NGC) and yields promising results for understanding ventricular tachycardia (VT) mechanisms during sinus rhythm. Indeed, by leveraging the activation morphologies and quantifying causal dependencies among neighboring signals, our method offers valuable insights into abnormal electrical wave propagation. Validation using simulated clinical data demonstrates its effectiveness in detecting anomalies and could thus improve treatment strategy design. Overall, this approach could enhance patient care in the management of VT.

References

[1] C. D. Cantwell, C. H. Roney, F. S. Ng, J. H. Siggers, S. J. Sherwin, and N. S. Peters, "Techniques for automated local activation time annotation and conduction velocity estimation in cardiac mapping," *Computers in biology and medicine*, vol. 65, pp. 229–242, 2015.

[2] B. S. Handa, X. Li, K. K. Aras, N. A. Qureshi, I. Mann, R. A. Chowdhury, Z. I. Whinnett, N. W. Linton, P. B. Lim, P. Kanagaratnam *et al.*, "Granger causality–based analysis for classification of fibrillation mechanisms and localization of rotational drivers," *Circulation: Arrhythmia and Electrophysiology*, vol. 13, no. 3, p. e008237, 2020.

[3] R. Cervigon, F. Castells, J. M. Gómez-Pulido, J. Perez-Villacastin, and J. Moreno, "Granger causality and jensen–shannon divergence to determine dominant atrial area in atrial fibrillation," *Entropy*, vol. 20, no. 1, p. 57, 2018.

[4] X. Shi, A. Sau, X. Li, K. Patel, N. Bajaj, M. Varela, H. Wu, B. Handa, A. Arnold, M. Shun-Shin *et al.*, "Information theory-based direct causality measure to assess cardiac fibrillation dynamics," *Journal of the Royal Society Interface*, vol. 20, no. 207, p. 20230443, 2023.

[5] H. Lütkepohl, "Non-causality due to omitted variables," *Journal of Econometrics*, vol. 19, no. 2, pp. 367–378, 1982. [Online]. Available: https://www.sciencedirect.com/science/article/pii/0304407682900112

[6] ——, *New Introduction to Multiple Time Series Analysis*. Springer, 2005. [Online]. Available: https://EconPapers.repec.org/RePEc:spr:sprbok:978-3-540-27752-1

[7] S. Basu, A. Shojaie, and G. Michailidis, "Network granger causality with inherent grouping structure," *Journal of Machine Learning Research*, vol. 16, no. 13, pp. 417–453, 2015. [Online]. Available: http://jmlr.org/papers/v16/basu15a.html

[8] H. Zou, "The adaptive lasso and its oracle properties," *Journal of the American statistical association*, vol. 101, no. 476, pp. 1418–1429, 2006.

[9] L. Zoroddu, P. Humbert, and L. Oudre, "Learning network granger causality using graph prior knowledge," *Transactions on Machine Learning Research*, 2024. [Online]. Available: https://openreview.net/forum?id=DN6sut5fyR

[10] S. Diamond and S. Boyd, "Cvxpy: A python-embedded modeling language for convex optimization," *Journal of Machine Learning Research*, vol. 17, no. 83, pp. 1–5, 2016.

[11] A. A. Cook, G. Mısırlı, and Z. Fan, "Anomaly detection for iot time-series data: A survey," *IEEE Internet of Things Journal*, vol. 7, no. 7, pp. 6481–6494, 2019.

[12] S. Coveney, C. Cantwell, and C. Roney, "Atrial conduction velocity mapping: clinical tools, algorithms and approaches for understanding the arrhythmogenic substrate," *Medical & Biological Engineering & Computing*, vol. 60, no. 9, pp. 2463–2478, 2022.

[13] B. Abdi, R. C. Hendriks, A.-J. van der Veen, and N. M. de Groot, "A compact matrix model for atrial electrograms for tissue conductivity estimation," *Computers in biology and medicine*, vol. 107, pp. 284–291, 2019.

[14] ——, "Improved local activation time annotation of fractionated atrial electrograms for atrial mapping," *Computers in Biology and Medicine*, vol. 117, p. 103590, 2020.

[15] B. Kölling, B. Abdi, N. M. de Groot, and R. C. Hendriks, "Local activation time estimation in atrial electrograms using cross-correlation over higher-order neighbors," in *2020 28th European Signal Processing Conference (EUSIPCO)*. IEEE, 2021, pp. 905–909.

[16] E. A. Nadaraya, "On estimating regression," *Theory of Probability & Its Applications*, vol. 9, no. 1, pp. 141–142, 1964.

[17] A. P. Bradley, "The use of the area under the roc curve in the evaluation of machine learning algorithms," *Pattern recognition*, vol. 30, no. 7, pp. 1145–1159, 1997.